PAPER

Check for updates

Synergistic impact of nano-supramolecular coordination polymer based on cadmium, ethyl nicotinate and thiocyanate ligands as efficient catalyst to remove harmful elements from wastewater†

Dalia I. Saleh, [ID] [a] Samy F. Mahmoud [ID] [b] and Safaa Eldin H. Etaiw [ID] *[c]

Under ultrasonication, cadmium nitrate tetrahydrates, ethyl nicotinate (EN), and potassium thiocyanate as connecting ligand self-assembled to form the nanosized supramolecular coordination polymer (NSCP**1**) and the crystalline supramolecular coordination polymer (SCP**1**) [Cd(EN)$_2$(SCN)$_2$]. Single crystal SCP**1** X-ray diffraction (XRD) revealed that Cd^{II} has an octahedral shape. The network structure of SCP**1** is composed of chair conformation cyclic [Cd$_2$(SCN)$_2$]$_n$ building blocks that form a one dimensional (1D) chain with bilaterally coordinated EN. The 1D-chain is joined to the other by extensive hydrogen bonds, which arrange the chains into a three-dimensional network. By stacking $\pi-\pi$, the strands are fluttering the three-dimensional (3D) network even more. Several structural characterization methods and spectral analyses were used to analyze SCP**1** and NSCP**1**. The heterogeneous catalysts SCP**1** and NSCP**1** have been shown to display exceptionally strong catalytic activity against the breakdown of the designated contaminant, indigo carmine (IC) color in very short durations under ultraviolet (UV) or ultrasonic wave conditions. The photoluminescence probing approach was utilized to determine the reactive oxygen species and reaction process using the disodium salt of terephthalic acid.

1 Introduction

In general, self-assembly of supramolecular coordination polymers (SCP) is a novel class of structures that may be put together from tiny components through peculiar noncovalent interactions. Lehn[1] defined the relatively new concept of SCP's comprehensibility in 1990. In optimal circumstances, SCPs exhibit the finest qualities of covalent polymers in addition to their unique reversibility, stability, responsiveness, and adaptability. As a result, they draw attention as green systems with a wide range of applications, including drug delivery, molecular devices, sensors, catalysis, and cell recognition.[2]

Noncovalent interactions[3] such as metal coordination,[4] hydrogen-bonding,[5,6] charge transfer effects, electrostatic interactions, $\pi-\pi$ interactions,[7,8] host–guest recognition,[9–12] ionic attraction,[13,14] and van der Waals forces[15,16] are the driving forces that are used to create SCPs. The knowledge and selection of noncovalent interaction can have a big impact on the SCP's structures. Noncovalent interactions' dynamic nature greatly influences their properties, which include some uncommon but also common traits including self-healing, simple processing, and stimulus responsiveness, in addition to the fundamental traits of conventional polymers.[17–22]

Self-assembly mechanisms are common in nature, where varying numbers of subunits can assemble into an ordered structure on their own to reduce systematic energy through local interactions between the subunits.[23–26] Particularly, many natural systems' self-assembly processes are designed with extreme care to ensure that the subunits are placed in a quasi-equilibrium fashion.[27,28] They can transform into many meta-stable intermediates to form the ultimate thermodynamic-stable state, and they are very sensitive to external stimuli due to the intricate interplay and delicate balance between different subunits.[29,30]

A variety of methods can be used to create supramolecular coordination polymers, such as microwave,[31] slow evaporation method,[32] slow diffusion,[33] hydrothermal approach,[34] mechanochemical synthesis,[35] ion-thermal synthesis,[36] and sonochemical technique.[37,38] The process that is thought to be most frequently used to produce SP is called solvothermal reactions. This process requires a lot of time, as well as high

[a]Department of Chemistry, College of Science, Taif University, P.O. Box 11099, Taif 21944, Saudi Arabia. E-mail: dalia.e@tu.edu.sa

[b]Department of Biotechnology, College of Science, Taif University, P.O. Box 11099, Taif 21944, Saudi Arabia. E-mail: s.farouk@tu.edu.sa

[c]Department of Chemistry, Faculty of Science, University of Tanta, 31527-Tanta, Egypt. E-mail: safaaetaiw@hotmail.com; safaaetaiw@science.tanta.edu.eg

pressure and temperature.[39] As an alternative, the sono-chemical method has been employed recently to produce a variety of submicron and nano-SP with the ideal and necessary diameters. The process is easy, quick, inexpensive, gentle, and moderately harmful to the environment.[40] A liquid experiences cavitation, which causes bubbles to form and then spontaneously collapse. This reaction results in a variety of supramolecular designs that are both nano- and submicron-sized.[41] Therefore, under these circumstances, extremely high pressure and temperature can lead to the formation of central spots of heat with microsecond lifetimes.[42,43]

The modes and different types of organic compounds play an efficient role in the structure of SCP.[44] The carboxylic pyridine acids represent the attractive multifunctional building blocks for creating SCP exhibiting fascinating structures.[45] Nicotinic acids are extremely important because they contain oxygen and nitrogen donor sites giving structures with divers' architectures.[46]

Ultrasonication is a unique homogenized technique used in various applications. Sonication usually breaks large particles in the fluid into smaller fragments or to uniform sized particles.[47,48] The production of nanoparticles can be achieved by providing sound energy to agitate the nanoparticles in the fluid.[49–51] Heat transmission in nanofluids will be enhanced by the ultrasonic effect. So, the preparation method depends on the ultrasonication time and the used power. However, it is unclear just how much time and power must be spent ultrasonically to produce nanoparticles.

Currently, there is a notable focus on developing highly effective and ambitious light-driven catalysis to treat environmental pollution, as there is an intense desire for a "green life". Chemical pollutants, which typically include paints, herbicides, dyes, detergents, fertilizers, and petroleum hydrocarbons, are among the thousands of pollutants found in the environment. There are numerous chemical compounds in each category. For instance, the textile and dyeing industries regularly utilize more than 100 000 synthetic dyes that are sold commercially.[52] More than 105 tons of industrial wastewater are produced by these dyes each year, and they are dumped straight into lakes, rivers, streams, and even the ocean. The majority of them are frequently persistent, poisonous, and non-biodegradable.[53,54] The most effective techniques for treating industrial waste streams are adsorption, precipitation, and coagulation, which are frequently employed in industrial laboratories.[55] Due to their inability to remove or destroy organic pollutants and their inefficiency when it comes to handling wastewater with low concentrations of organic pollutants, these conventional approaches may have certain drawbacks.[56] To solve this, it's essential to create a cutting-edge oxidation process that is easy to use, quick, affordable, and efficient for eliminating these hazardous substances from water sources. To address this, it is critical to develop an advanced oxidation method that is simple, rabid, inexpensive, and effective for removing these dangerous compounds from water supplies.

The goal of this research is to synthesize new single crystals of SCP1, which includes ligands for thiocyanate, ethyl nicotinate, and cadmium. Additionally, the work synthesizes a new nano-SCP1 comprising the same compounds using ultrasonic waves. The X-ray diffraction of single crystals was employed to investigate the structures of SCP1 and NSCP1, in conjunction with spectrophotometric and physical data. To assess the catalytic activity of 1, indigo carmine was utilized as a typical example, Scheme S1.†

2 Experimental

2.1 Chemicals and equipment

Chemicals utilized in this research work are of high purity which had been purchased from Sigma-Aldrich and had been used as received. Spectroscopic grade BDH organic solvents were used. The starting concentration of H_2O_2 (Merck, 30% w/v) had been estimated iodometric ally. Equipment and physical measurements are as previously described.[57]

Crystal structure of single crystals of SCP1 was recorded utilizing the four-circle goniometer Kappa CCd Enraf Nonius FR 90 with graphite monochromatic MoKα radiation $\{[\lambda_{MoK\alpha}] = 0.71073 \text{ Å}\}$ 30 °C. Direct methods were used to solve the structure of 1 and the atoms except hydrogen are fixed at the beginning of measurement starting from the first steps of refinement. Mercury 3.8 software had been utilized for structure visualizations. The refinement parameters of NSCP1 are present in Table S1.†

2.2 Syntheses of the crystals of $[Cd(EN)_2(SCN)_2]_n$ (SCP1) and the nano-particles of NSCP1

An agitated solution containing (2 mmol, 0.302 gm) of EN was gradually mixed with $CdSO_4 \cdot 4H_2O$ (0.280 gm, 1 mmol) aqueous solution at room temperature. After a few minutes of vigorous stirring, 5 mL of a potassium thiocyanate water solution (2 mmol, 0.194 g) was added dropwise to the mixture, and another few minutes of vigorous stirring were required. After a few days, the solutions were allowed to gradually evaporate, producing white crystals of SCP1 (556 mg, 70% yield). Conversely, the combination of the aforementioned substances and amounts were exposed to 70 W of ultrasound power (Power sonic 405 with output 350W – Hwashin Co.) for three hours to afford the colorless nanoparticles of the nano-supramolecular coordination polymer NSCP1. Anal. calc for SCP1 ($C_{18}H_{18}N_4O_4S_2Cd$); C, 40.72; H, 3.42; N, 10.55%. Found: C, 40.79; H, 3.59; N, 10.48%.

2.3 Measurements of catalytic and photocatalytic activity

The degradation of indigo carmen (IC) in the presence of H_2O_2 was used to measure the catalytic and photocatalytic activity of the produced SCP1 and NSCP1. Typically, 7.0×10^{-5} M IC dye aqueous solution was mixed with 25 mg of the title compounds and 0.1 M H_2O_2 which had been magnetically stirred at ambient conditions to guarantee (IC) deterioration. Subsequently, the identical component was exposed to UV-light using a lamp with a wavelength of 365 nm. Using a magnetic stirrer, the solution was continually stirred throughout the irradiation procedure. To assess the impact of sonication on the degradation of IC dye, the reactor was additionally placed in an ultrasonic bath
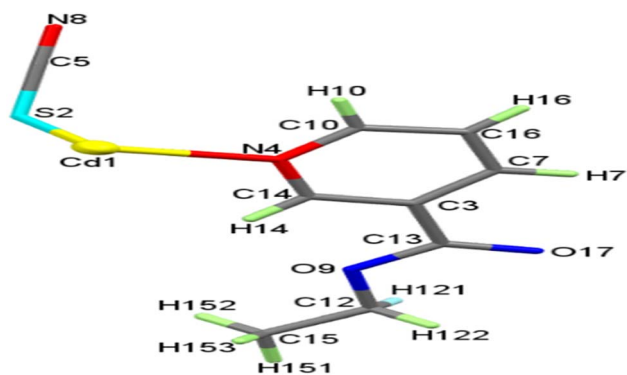
Fig. 1   A symmetric unit of SCP1 with atom labeling scheme.

equipped with a 60 W ultrasonic generator. Following that, a transparent sample solution of 5 mL was taken from each jar and analyzed using spectrophotometry while the decolorization was calculated using the following equation:

$$D\% = \frac{(A_0 - A_t)}{A_0} \times 100 \qquad (1)$$

where initial and remnant absorbances were represented by A_0 and A_t of the dye at times 0 and t, respectively.

3   Results and discussion

3.1   Crystal structure of $[Cd(EN)_2(SCN)_2]_n$ (SCP1)

At room temperature, the reactions of aqueous Cd^{2+} cation with ethyl nicotinate (EN) and KSCN produced a Cd^{II} complex of the form $[Cd(SCN)_2(EN)_2]$, SCP1. When properly dried, the SCP1 is sufficiently stable against air-oxidation, diamagnetic, and colorless. It is easily soluble in DMF but insoluble in a wide range of typical polar and non-polar solvents, including water, methanol, ethanol, acetone, and benzene. With two formula units in the unit cell, Table S1,† Within the monoclinic space group $P2_1/c$, the SCP1 crystallizes. One Cd atom, one thiocyanate anion, and one ethyl nicotinate ligand in general positions make up the asymmetric unit of 1, as shown in Fig. 1, whereas the ORTEP diagram has 2 repeating asymmetric units showing the coordination environment of cadmium. Cd1 atom has an octahedral shape and is coupled to two S-bonds, two N-bonds, and two N atoms of EN ligands from four *trans*-oriented 1,3-μ^2-SCN^- anions, Fig. 2. On the other hand, the SCP1's structure is composed of cyclic building units $[Cd_2(SCN)_2]_n$ that display chair conformation, forming a 1D chain that is adorned with coordinated EN on both sides, Fig. 3. As shown in Fig. 3 and Table S2,† the CdN_4S_2 octahedral is slightly deformed, with distances between 2.377 Å and 2.734 Å and angles between
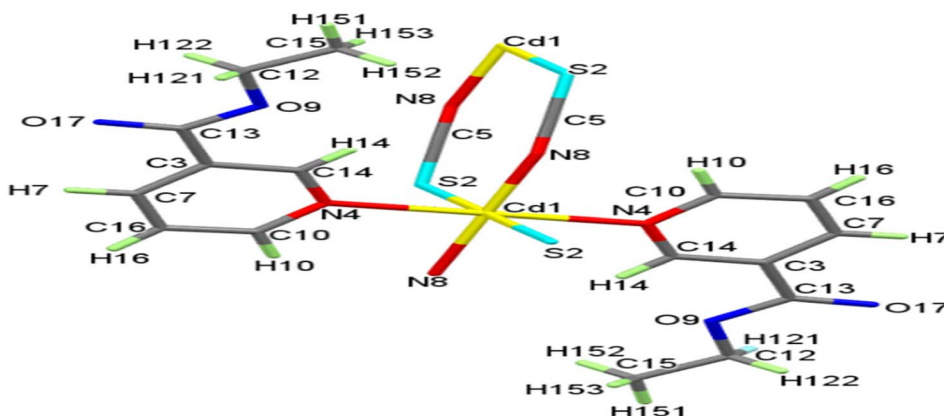

Fig. 2   The ORTEP plot of SCP1 with atom labeling scheme showing the coordination geometry of cadmium.
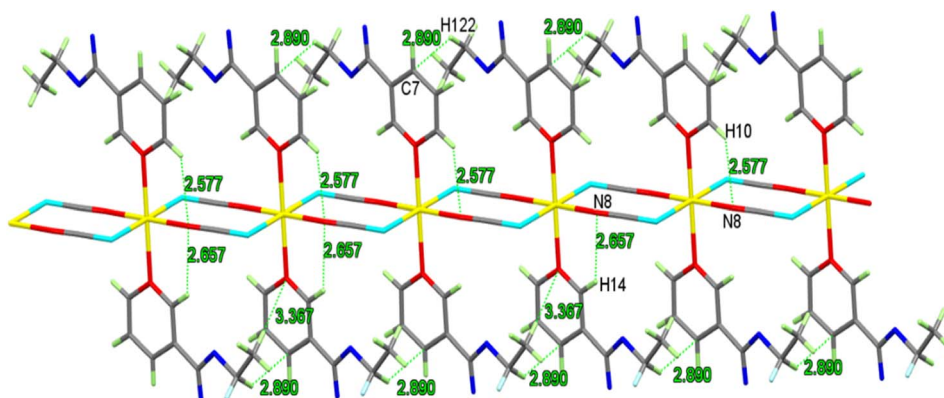

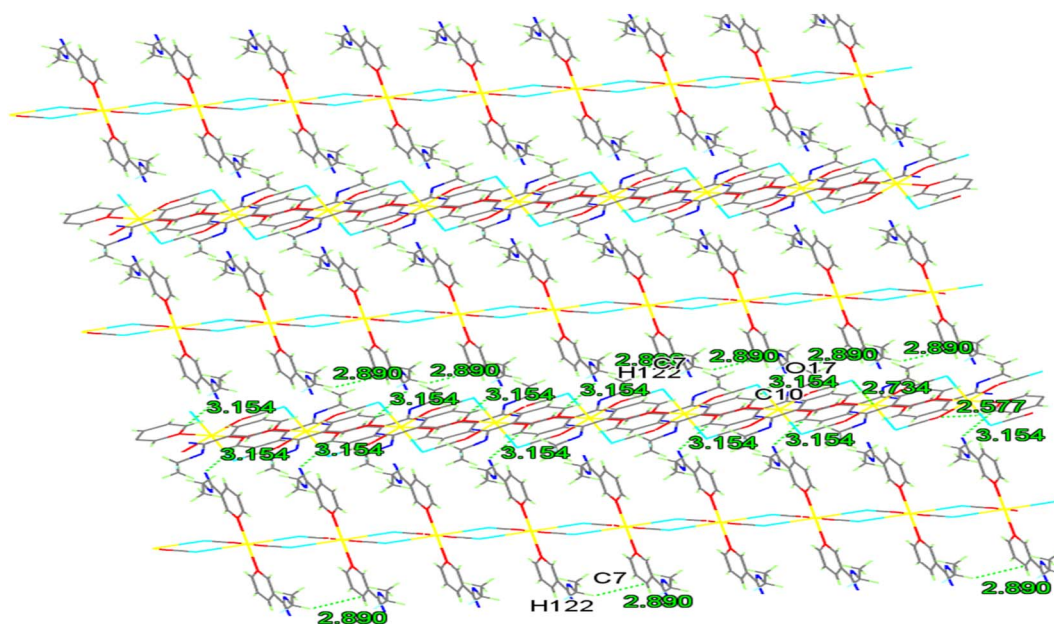Fig. 3   Visualizations of 1D-chain of SCP1 along *b*-axis showing H-bonds.

Fig. 4 Visualization of 2D-layer of SCP**1** along *a*-axis showing H-bonds.

88.33° and 91.67° and 180°. Table S2† shows that the S(2)–C(5)–N(8) bond angle is 179.15°, indicating that the SCN$^-$ group is nearly linear. With bond angles of 164.30° and 100.06° for C(5)–N(8)–Cd(1) and C(15)–S(2)–Cd(1) respectively, the Cd(ɪɪ) and SCN$^-$ groups suffer bent structures. Similar values have been reported for comparable complexes.[58–60]

Adjacent Cd atoms are joined by two 1,3-μ^2-SCN$^-$ anions to form an infinite polymeric 1D-chain with a Cd···Cd distance of 5.926 Å, Fig. 4. Extensive structural analyses revealed that the one-dimensional chain is connected to the other by hydrogen bonds formed between the oxygen or carbon atoms of EN in one chain and the hydrogen atoms of EN ligands in another chain, forming a two-dimensional (2D) layer, Table S3† and Fig. 4.

Moreover, 2D layer is formed by the 1D-chains being compressed along the *a*-axis like a spring. The strands are further flapping the 3D-network by π–π stacking (3.47–3.64 Å) and H-bonds (2.43–2.89 Å), as seen in Fig. 5 and Table S3.†

3.2 Morphology and particle size of NSCP1

Transcriptome analysis utilizing Transmission Electron Microscopy (TEM) exhibiting high resolution is used to measure the shape and the size of particle of **1**, seeing Fig. 6. NSCP**1**'s high magnification transmission electron microscopy images show homogeneous circular-morphology nanostructures with an excellent distribution of particle sizes between 9.74 and
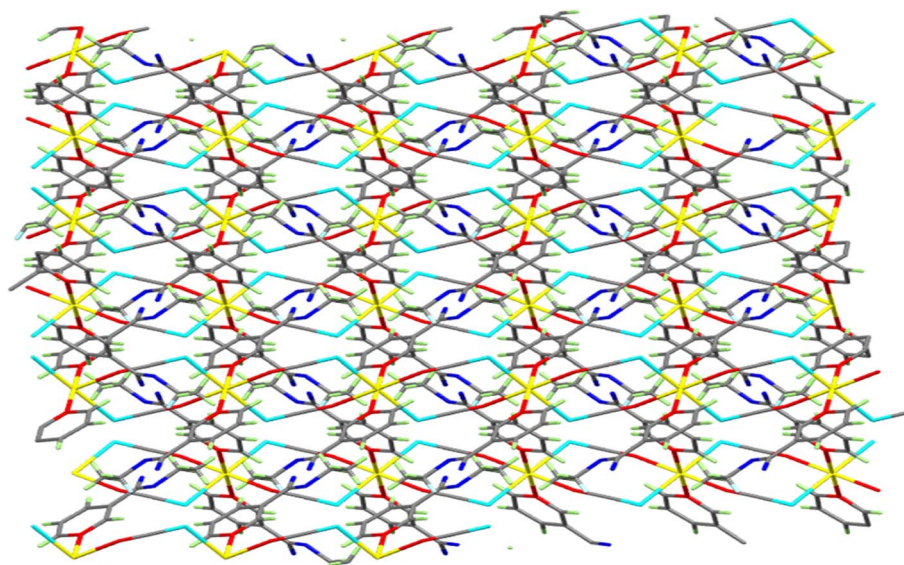

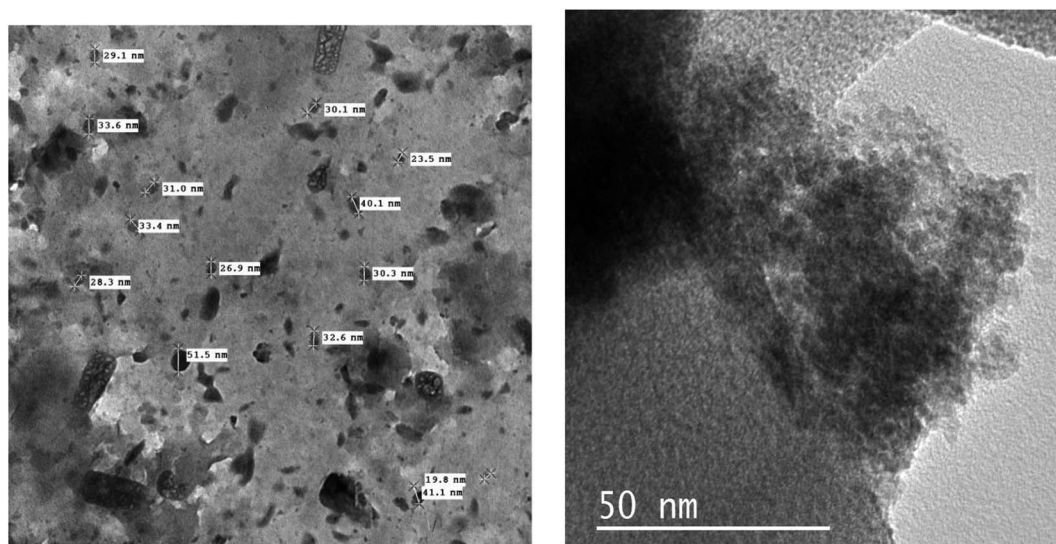**Fig. 5** View of the 3D-network of SCP**1** along the *c*-axis.

Fig. 6   TEM images of NSCP**1**.

32.63 nm. The distribution of the particle and cavity diameters was estimated using histograms (Fig. 7), which can offer an overall approximation of the probability distribution of a continuous series of varying cavity and nanoparticle dimensions. The area of the bar indicates how frequently each nanoparticle occurs, Fig. 7. The average cavity size is 55 ± 20.5 nm, while the average size of the nanoparticles is 28.33 ± 17.5 nm.

3.3   Spectroscopic and thermal studies of NSCP1

The bands of the EN and thiocyanate ligands are seen in the NSCP**1**'s infrared (IR) spectrum, Fig. S1.† EN displays bands of $v\text{CH}_{\text{arom}}$ at 3036 cm^{-1}, $v\text{CH}_{\text{aliph}}$ at 2990, 2917 cm^{-1}, δCH at 1410 cm^{-1}, and γCH at 790 and 770 cm^{-1}. The establishment of hydrogen bonds causes these bands to be moved from the vibrational frequencies of the unbound ligand to lower wave numbers. Apart from the band at 862 cm^{-1} caused by the $v_{(CS)}$,[61] the thiocyanate ligand's $v_{(CN)}$ mode is shown by a strong absorption band at 2093 cm^{-1}. The NCS bending modes are visible at 474 cm^{-1}. Additionally, the trans disposition of the thiocyanate groups in NSCP**1** is indicated by the non-splitting of the CN stretching band.[62,63] The sharp band at 1721 cm^{-1} is associated with the NSCP**1**'s C=O, which moves to a lower wave number because of hydrogen bond formation than the free ligand's $v\text{C} = \text{O}$ (1738 cm^{-1}). The IR spectrum of **1** shows a shift to lower values in the band at 1610 cm^{-1}, which corresponds to stretching vibrations of (C=N) of the ligand EN. The lone pair density of the azomethine nitrogen moving towards the core metal atoms can account for this shift.[64] This implies that the
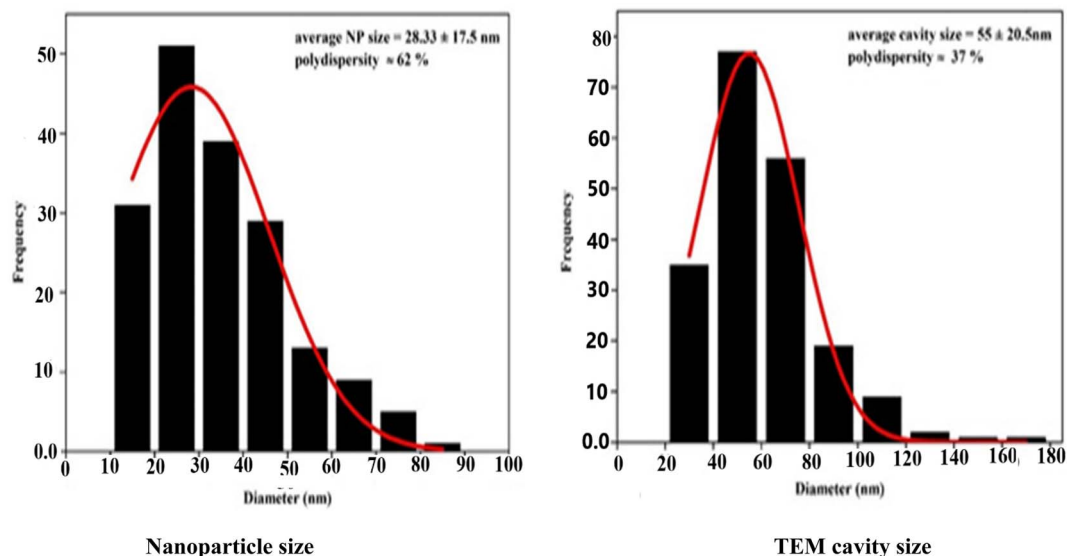

Fig. 7   The symmetric unimodal histograms show the average nanoparticles and pores size for NSCP**1**.

Table 1   Thermogravimetric data of NSCP1

| No | Temp. range (°C) | Mass loss (%) | | Assignment |
		Found	Calc.	
NSCP1	53–110	5.59	5.47	Loss of $C_2H_5O_2$
	110–200	52.76	51.47	Loss of $C_{14}H_{13}N_2O_4$
	204–400	15.29	15.84	Loss of SCN and CN
	400–700	27.12	27.22	Formation of CdS

source of coordination is the (C=N) nitrogen atom. The stretching vibrations of the aromatic C=C exhibit bands at 1560, 1468, and 1412 cm^{-1}. The $\nu_{(Cd-S)}$ metal sulfur bond band is located at 463 cm^{-1}, and the $\nu_{(Cd-N)}$ vibrations are responsible for the band at 485 cm^{-1}.

Three absorption bands were visible in the electronic absorption spectra of 1 and EN ligand. The pyridine ring's $^1La \rightarrow {}^1A$ and $^1Lb \rightarrow {}^1A$ are attributed to the two bands of EN at 210 nm and 258 nm, respectively.[65] These bands show a red shift in the spectra of 1, Fig. S2.† The spectrum of 1 shows that the third absorption band at 314 nm in the spectrum of EN is caused by n–π*, which vanishes indicating that EN is coordinated with the metal ion. LMCT is shown by the third absorption band of 1 at 348 nm.

Furthermore, because d^{10} metal coordination compounds have outstanding luminous characteristics, the photoluminescence (PL) spectrum of 1 has been studied in the solid state.[66–68] At ambient temperature, the EN ligand's emission spectra exhibits no bands upon excitation at 290 nm. Given that pyridine and its derivatives are often not luminous materials, this result is expected.[69] In contrast, SCP1 and NSCP1's emission spectra show a broad band around 470 nm when excited at 340 nm, Fig. S3.† The NSCP1 emission is not indicative of either ligand-to-metal transfer (LMCT) or metal-to-ligand charge transfer (MLCT) because of the difficulty in oxidizing or

reducing the Cd^{2+} ion because of its d^{10} structure.[70–72] The emission of 1 could be a combination of ligand-to-ligand charge transition (LLCT) and intra-ligand characteristics, primarily transition from π → π* inside the coordinated EN ligands.[73,74] When the metal ions coordinate with the organic ligands, the conjugated system increases, which is responsible for the greater PL intensities of 1. Organic ligands and metal ions together efficiently boost the ligand's conformational stiffness and decrease energy loss through vibration motions.[75,76]

Three breakdown phases are displayed in the thermal gravimetric analysis (TGA) curve of the NSCP1, Table 1 and Fig. S4.† The first stage of NSCP1 took place between 53 and 110 °C and had a mass loss of 5.59% (cal. 5.47%), which is equivalent to the ethyl group [C_2H_5] being eliminated. The removal of the EN group and the nicotinate group [$C_{14}H_{13}N_2O_4$] occurs in the second step, which occurs between 110 and 200 °C and has a mass loss of 52.76% (cal. 51.47%). The removal of SCN and CN groups [C_2H_2S] is represented by the third phase, which occurs at around 204–400 °C and has a mass loss of 15.29% (cal 15.84%). The final product, CdS, is the residual portion.

3.4 Catalytic and photo-catalytic activities of SCP1 and NSCP1

The catalytic behavior of SCP1 and NSCP1 was studied in the presence of H_2O_2 as an ecologically acceptable environment, using the dangerous color indigo carmine (IC) as an example. This dye is stable in typical environmental circumstances and difficult for waste streams to break down. The deterioration tests are tracked using the IC dye spectrum at 612 nm. The spectra under UV radiation only show no significant drop in the intensity of the unique band even after lengthy times 12 h. On the other hand, the preliminary tests of the spectra, conducted without the use of the tested catalyst but within the proximity of H_2O_2 in dim exhibit $D\% = 51.62\%$ within 11 h, Fig. S5.† The
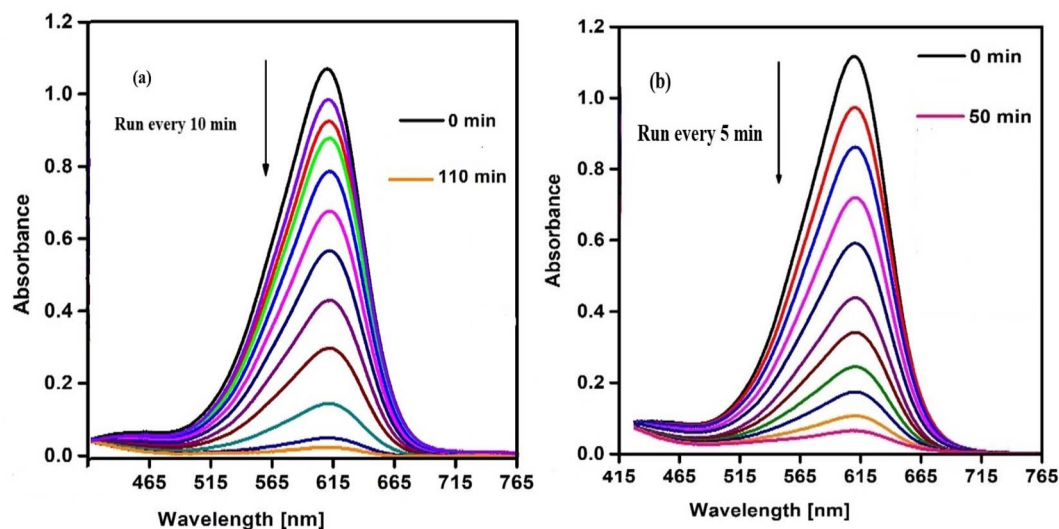

Fig. 8 . Catalytic spectra of degradation the IC dye solution (7.0×10^{-5} M) and (0.1 M) H_2O_2 and (0.025 g) catalyst normal conditions at pH = 6 (a) catalyst SCP1 (b) catalyst NSCP1.
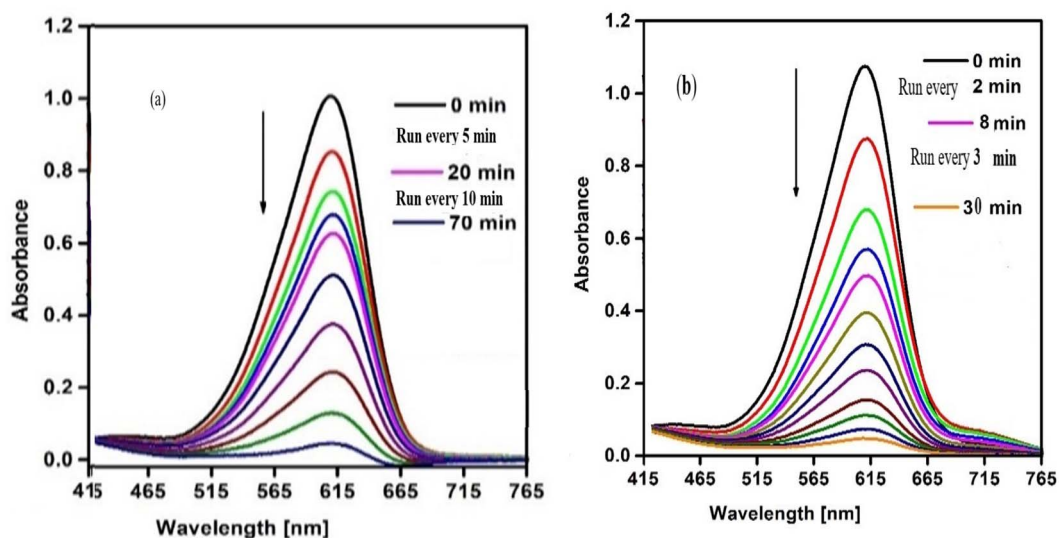
Fig. 9 Catalytic spectra of degradation the IC dye solution (7.0×10^{-5} M) and (0.1 M) H_2O_2 and (0.025 g) catalyst under UV-light at pH = 6 (a) catalyst SCP**1** (b) catalyst NSCP**1**.

presence of a catalyst activates H_2O_2, leading in the formation of the effective hydroxy radical (HO˙), an aggressive oxidant species.[34–37] So, it is evident that the IC dye solution does not deteriorate considerably in the absence of a catalyst. In this case the degradation of IC dye takes place in the presence of SCP**1** or NSCP**1** and H_2O_2 at PH = 6 (normal conditions), Fig. 8, while in addition to that applying UV or ultrasonic waves, the intensity of the absorption peaks dramatically decrease, Fig. 9 and 10. In the case of SCP**1**, $D\% = 98.42$ (110 min), $D\% = 98.88$ (70 min), 98.72 (45 min), and for NSCP**1**, $D\% = 98.14$ (50 min), 97.21 (30 min), and 96.24 (22.5 min), applying normal conditions, UV-radiation and ultrasonic waves, respectively.

The pseudo-first order approach was used for the kinetic investigations, and the results showed that the $[H_2O_2]_0$ was at least ten times higher than the $[dye]_0$. The first-order plot slope was used to compute the observed rate constant, or k_{obs}, which supports eqn (2).

$$\ln A_t = \ln A_0 - k_{obs} \times t \ \text{ or } \ \ln \frac{A_0}{A_t} = k_{obs} \times t \qquad (2)$$

The absorbances at times = t and zero are represented by A_t and A_0, respectively. Table 2, and the findings support pseudo first-order rate with respect to dye concentration. The relationship yields the particular rate constant,

$$k = k_{obs}/[H_2O_2]_0.$$

By utilizing the decrease in the dye solution's absorption intensity, the percentage of color removal ($R\%$) is calculated, eqn (3).
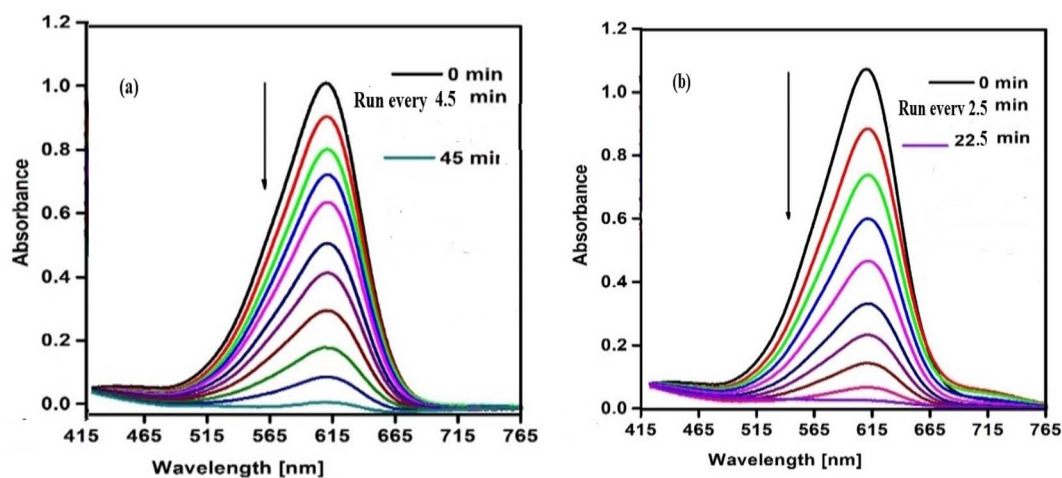

Fig. 10 Catalytic spectra of degradation the IC dye solution (7.0×10^{-5} M) and (0.1 M) H_2O_2 and (0.025 g) catalyst under ultrasonic waves at pH = 6 (a) catalyst SCP**1** (b) catalyst NSCP**1**.

Table 2 Kinetic parameters of catalytic degradation of IC dye using SCP**1** and NSCP**1** catalysts[a]

System	$D\%$	Time (min)/(h)	k_{obs} (min^{-1})	R^2	k (L mol^{-1} min^{-1})
pH = 6					
IC + UV-light	11.20	12 (h)	0.0015	0.991	0.015
IC + H$_2$O$_2$	51.6	11 (h)	0.002	0.990	0.020
IC + SCP**1** + H$_2$O$_2$ + (NC)	98.20	110	0.026	0.987	0.260
IC + SCP**1** + H$_2$O$_2$ + UV-light	98.88	70	0.033	0.976	0.330
IC + SCP**1** + H$_2$O$_2$ + ultrasonic waves	98.87	45	0.062	0.987	0.620
IC + NSCP**1** + H$_2$O$_2$ (NC)	98.14	50	0.087	0.997	0.870
IC + NSCP**1** + H$_2$O$_2$ + UV-light	97.21	30	0.094	0.986	0.940
IC + NSCP**1** + H$_2$O$_2$ + ultrasonic waves	96.24	22.5	0.113	0.983	1.130
pH = 9					
IC + SCP**1** + H$_2$O$_2$ (NC)	98.51	20	0.168	0.996	1.680
IC + SCP**1** + H$_2$O$_2$ + ultrasonic waves	98.87	12	0.279	0.993	2.790
IC + NSCP**1** + H$_2$O$_2$ (NC)	98.09	6	0.510	0.994	5.100
IC + NSCP**1** + H$_2$O$_2$ + UV-light	98.83	6	0.672	0.989	6.720
IC + NSCP**1** + H$_2$O$_2$ + ultrasonic waves	99.45	5	0.702	0.983	7.020

[a] (NC) = normal conditions.

$$R\% = \frac{(C_0 - C_t)}{C_0} \times 100 \qquad (3)$$

The dye's absorbance at periods 0 and t is denoted by C_0 and C_t, respectively.

Even though a variety of factors affect declining efficiency. The pH of the solution and the concentration of H$_2$O$_2$ are the most crucial factors. In order to maximize the catalyst's performance, we must investigate the optimal parameters. Therefore, to ascertain the optimal parameters for IC dye mineralization utilizing the catalyst under consideration, the impacts of H$_2$O$_2$ concentration and solution pH have been studied.

The rate at which IC dye degrades is significantly influenced by the initial concentration of H$_2$O$_2$. At 0.05 M H$_2$O$_2$ concentration, the reaction rate increases to 1.6×10^{-2} min^{-1}; at 0.1 M [H$_2$O$_2$], it climbs to 8.9×10^{-2} min^{-1}. Following that, the starting H$_2$O$_2$ concentration was raised to 0.125 M, at which

point the reaction rate drops to $(3.4 \times 10^{-2}$ min$^{-1})$. This behavior supports Fig. 11(a) in showing that there is an optimal H$_2$O$_2$ dosage.

The pH is changed from 4 to 9 to examine how the pH affects the breakdown process. The degrading efficiency increases significantly, and the measured rate constantly rises from $(1.3 \times 10^{-2}$ min$^{-1})$ to $(50.2 \times 10^{-2}$ min$^{-1})$ when the reaction's pH is raised from 4 to 9. This is the cause of the IC dye's increased oxidation process. This trend suggests that there is a perfect pH, with pH = 9 being the ideal value; see Fig. 11(b).

The degradation studies were therefore conducted with ultrasonic waves and normal conditions with 0.025 gm catalyst, 7.0×10^{-5} M IC dye, and 0.1 M H$_2$O$_2$ at pH = 9: in the case of SCP**1**, Fig. 12(a, b) and Table 2, $D\%$ = 98.51 within 20 minutes and 98.87 within 12 minutes (ultrasonic waves). On the other hand, NSCP**1** exhibits the following degradation efficiencies: $D\%$ = 98.09 (normal condition), 98.83 (UV-radiation) in 6 minutes and 99.45 in 5 minutes (ultrasonic), Fig. 12(c and d).

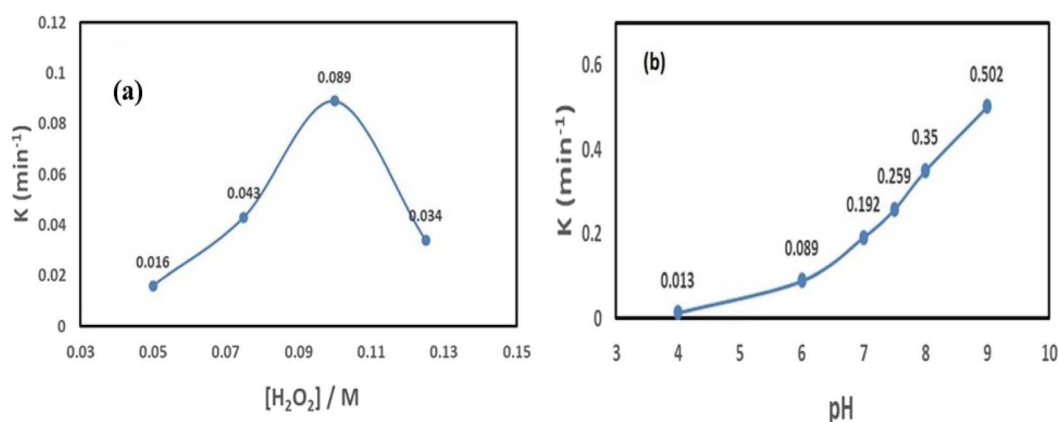**Fig. 11** Impact of operational parameters on the NSCP**1** catalyst and H$_2$O$_2$ as an oxidant-mediated catalytic degradation of the indigo, carmine dye (IC) solution where (a) effect of hydrogen peroxide concentration and (b) effect of pH of solution.
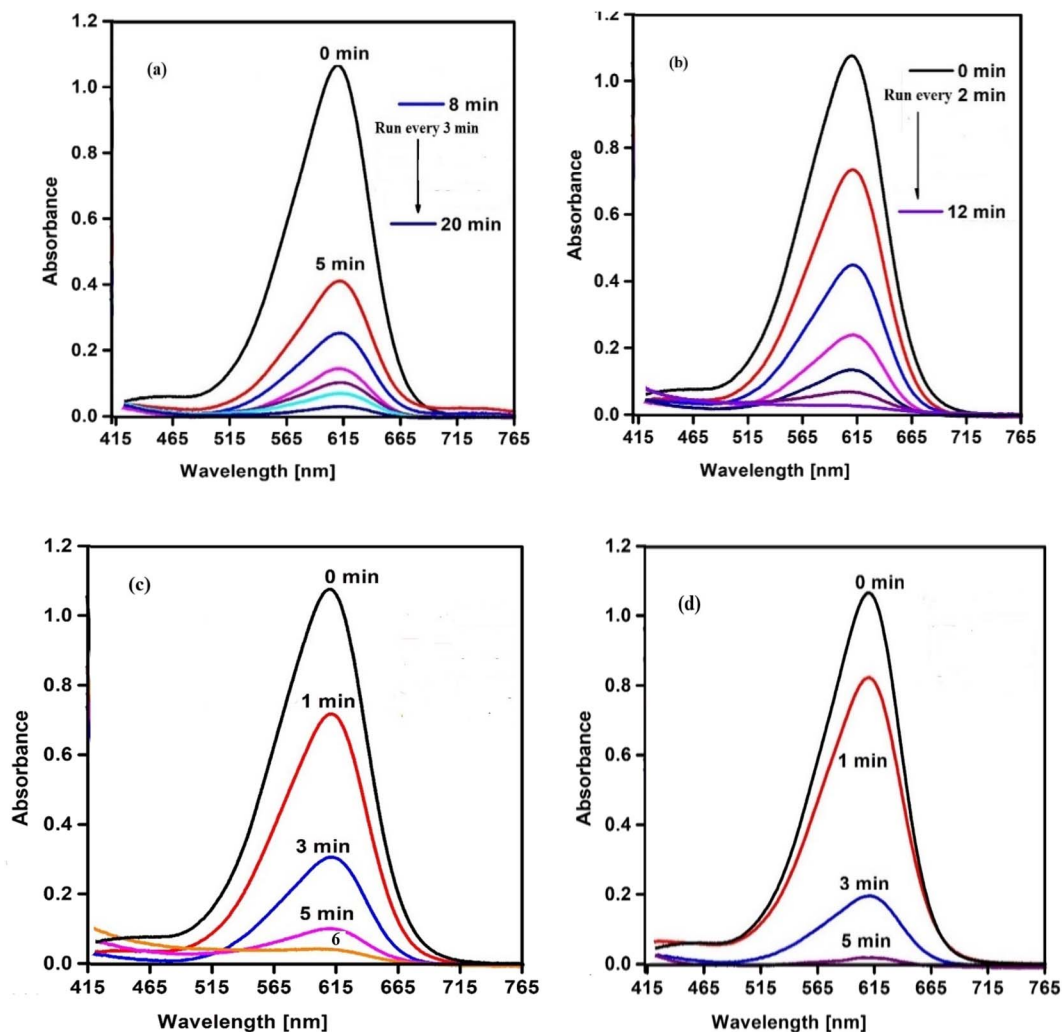
Fig. 12 Spectra of the catalytic degradation of the IC dye solution (7.0 × 10^{-5} M), H$_2$O$_2$ (0.1 M) and catalyst (0.025 g) at pH = 9, normal and ultrasonic irradiation, SCP**1** (a and b), NSCP**1** (c and d), respectively.

When H$_2$O$_2$ and ultrasonic vibrations are added, the NSCP**1** catalyst's deteriorating efficiency reaches its maximum value in a comparatively short amount of time. NSCP**1** has a higher energy for dye degradation in the experiment because of its small nanoparticle size.

3.5 Reuse and stability of the catalysts

The potential for catalyst recycling is a crucial consideration when researching liquid-phase oxidations over solid catalysts. Catalyst reuse can be evaluated by cleaning with deionized water, drying, and then testing again after the initial experiment is completed. Fig. 13 shows that the catalyst NSCP**1** can sustain its catalytic activity for six cycles of H$_2$O$_2$-mediated dye oxidation under typical conditions. The deterioration of efficiency time remains relatively unchanged after recycling, as it would in a typical circumstance. After degradation procedures, SCP**1** and NSCP**1**'s IR-band positions are the same as SCP**1**'s before degradation, as shown in Fig. S1† (*vide supra*), indicating that the catalysts under research are unaffected by H$_2$O$_2$ and retain their identities following degradation investigations.

The experimental XRPD graphs of NSCP**1** following degradation are shown in Fig. 14 and are followed by consulting the XRD simulated plot of SCP**1**. Consequently, there is good agreement between the experimentally powdered bulk samples before and after degradation with the simulated XRPD plot of the single crystals upon deterioration. The example that confirms they both have excellent stability, good phase purity, and structural similarity.

The catalyst was reused six cycles which show no significant changes in degradation efficiency (Fig. 13) indicating that the catalysts sustain their identity otherwise the degradation efficiency will be clearly affected. Also, XRPD and IR spectra of the catalysts after recycling (Fig. S1† and 14) indicated stability of the catalysts and suggested that the catalysts being studied are not impacted by the aqueous medium and maintain their identities after degradation studies. These heterogenous catalysts maintain their shape and color after degradation process. In addition, figures of IR and electronic absorption spectra of the mineralized dye solution (Fig. S6 and S7†) do not show any IR-peaks or UV-vis bands characteristic to the catalyst
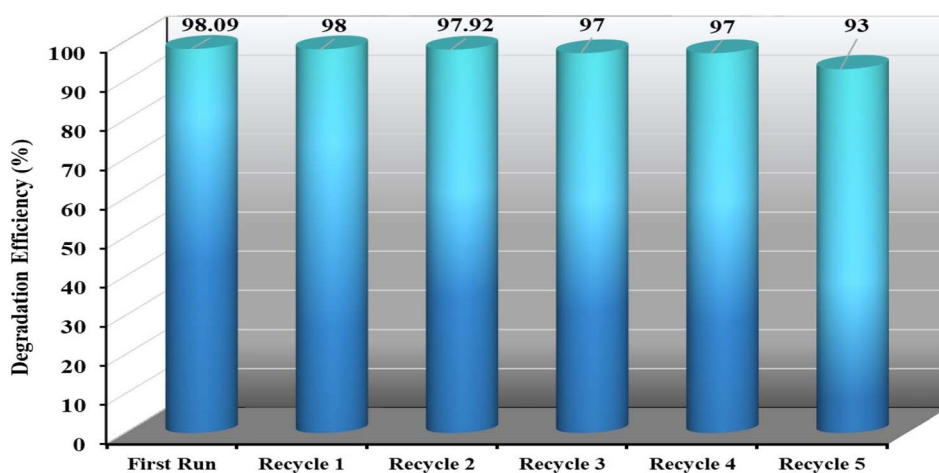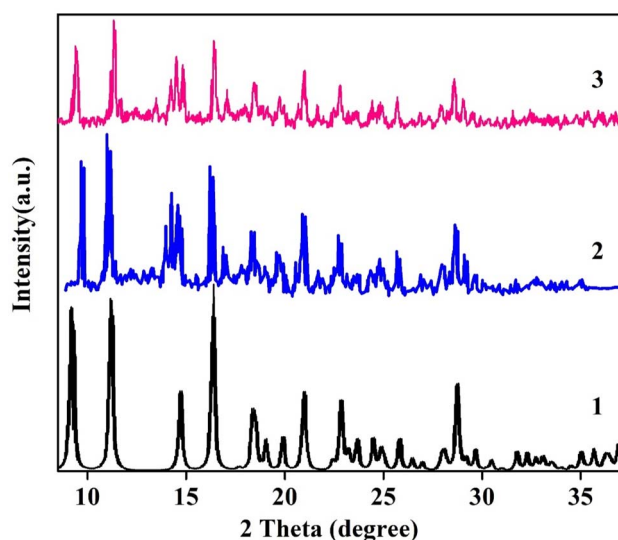
Fig. 13 Recycling of NSCP**1**.

Fig. 14 XPRD of **1** (SCP1-simulated), **2** (NSCP1), **3** (NSCP1-after recycling).

supporting that the mineralized dye solution is free of any catalyst fragments. This example demonstrates that the stability of [Cd(EN)$_2$(SCN)$_2$] supramolecular coordination polymer prevents any Cd leaching in the media. Furthermore, there are no IR peaks or UV-vis bands visible in the mineralized dye solution's, Fig. S6 and S7,† which indicate that the solution is completely devoid of catalyst fragments.

Two distinct concepts—thermodynamic stability and kinetic stability—can be used to describe the stability of metal complexes.[77,78] However, thermodynamic stability, or the absence of a reaction with water that would lower the system's free energy, characterizes a metal complex as stable. Since the [Cd(EN)$_2$(SCN)$_2$] supramolecular coordination polymer is thermodynamically stable and the XRPD and IR-spectra (see supra) do not show the presence of any types of Cd(OH)$_n^{2-n}$ hydroxide complexes in solution. So, Cd could not leach in the catalysis medium.

3.6 Analysis of degradation products

Apart from chemical methods, the products remaining in the solution after the IC dye has calcified are analyzed using FT-infrared and electronic spectra under standard conditions. The FT-IR spectra, Fig. S6,† show strong extending vibration peaks of NH, SO$_3^{2-}$, C=O, C=C, C–O, and C$_{Ar-N}$ in the infrared spectrum prior to the degradation of the IC dye. The absence of these peaks in the decolorized IC IR-spectrum confirmed the dissociation of the IC dye from the SO$_3^{2-}$ and CO groups and the rupture of the aromatic rings. Moreover, notable bands at 1630, 1500, 1420, and 1050 cm^{-1} can be observed; these are like the corresponding stretching vibrations of HNO$_3$, H$_2$SO$_4$, and CH$_3$COOH.[79] This suggests that the primary finished products are CO$_2$, H$_2$O, and certain acids. Contrasting the absorption spectra of the IC dye during the deterioration process also demonstrated that the dye was entirely destroyed by UV light and normal circumstances, as shown in Fig. S7.† The absorption peaks immediately decreased, demonstrating the speedy elimination of the IC dye and the aromatic system. The unreacted H$_2$O$_2$ is measured by iodometric means (2 × 10^{-5} M L^{-1}). The result of the interaction between CO$_2$ and the Ca(OH)$_2$ solution is CaCO$_3$, which weighs 0.0142 grams according to gravimetric measurements. By precipitation, the sulfate ions are measured gravimetrically as BaSO4 (0.0436 gram). Titrating is used to calculate the mixture's total acid concentration with sodium hydroxide (1.2 × 10^{-3} M L^{-1}).

3.7 Examining the catalytic processes' mechanism and active species

3.7.1 Hydroxyl radical determination. The formation of hydroxyl radicals (˙OH) on the catalyst surface was detected by the photoluminescence (PL) technique using terephthalic acid as a probe molecule.[80–82] Other reactive species including H$_2$O$_2$, HO$_2^\bullet$, and O$_2^{\bullet-}$ do not alter the reaction, hence it could be employed as a sensitive probe to find ˙OH radicals.[83] This helps to clarify which active species are involved in the catalytic process. The photogenerated 2-hydroxyterephthalic acid's PL

intensity gradually increases at around 425 nm over time showing the PL spectra for a solution of (0.05 M) terephthalic acid in (0.1 M) NaOH with NSCP1 present. Within 55 minutes, the intensity suddenly increases to 1000 nm, Fig. S8.† Nevertheless, the PL intensity drops and only rises to 160 nm in 90 minutes when IC dye is simultaneously added to the solution under the same circumstances, Fig. S9,† suggesting that some of the $\cdot OH$ radicals reacted with IC fast based on the discoloration observed during fluorescence measurements. It is important to note that, under the same testing conditions, the components of NSCP **1** do not exhibit any catalytic activity towards the breakdown of IC dye.

3.8 Examining the catalytic processes' mechanism and active species

In order to comprehend the role of the active species—primarily $\cdot OH$, h^+, and $O_2^{\cdot-}$ produced in the catalytic process, further research is being done on the existence of scavengers. Following exposure to the IC/H_2O_2/NSCP1 system, the mineralization efficiency of the IC dye decreased to 59.8% in 54 minutes, 68.8% in 73 minutes and 85.23% in 56 minutes, for IPA (isopropanol), BQ (benzoquinone), and AO (ammonium oxalate), respectively, Fig. 15. In this case, IPA, BQ and AO successfully quench the active species $\cdot OH$, h^+, and $O_2^{\cdot-}$, demonstrating that the catalytic process is influenced by the pace at which these active species are produced, Fig. 15.

These results allow for the proposal of a mechanism involving the reaction between the catalyst being tested and H_2O_2 that results in the generation of extremely active oxidizing species, primarily $\cdot OH$ radicals.

$$H_2O_2 + [NSCP1\ Cd^{II}] \rightarrow \cdot OH + OH^- + [NSCP1\ Cd^{III}] \quad (4)$$

$$OH^- + [NSCP1\ Co^{III}] \rightarrow [NSCP1\ Co^{II}(OH)] \leftrightarrow$$
$$[NSCP1\ Co^{II}] + \cdot OH \quad (5)$$
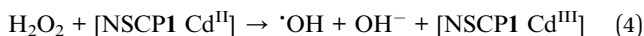
Hydroxyl radicals fuel the process by reacting with the IC dye to produce degradation products.

$$\cdot OH + IC\ dye \rightarrow intermediates \quad (6)$$

$$Intermediates \rightarrow oxidation\ products + CO_2 + H_2O \quad (7)$$
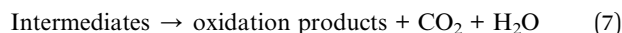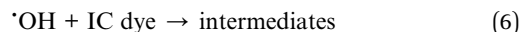
It is also possible to have a lot of other reactions, including the radical–radical reaction or the reaction of the $\cdot OH$ with H_2O_2.

$$\cdot OH + \cdot OH \rightarrow H_2O_2 \quad (8)$$

$$\cdot OH + H_2O_2 \rightarrow \cdot OOH^- + H_2O \quad (9)$$
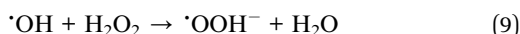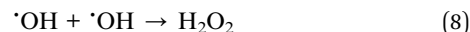
Peroxide radicals ($HO_2^{\cdot-}$) could oxidize other species present in the solution.[84]

$$\cdot OOH^- + [NSCP1\ Cd^{II}] \rightarrow O_2 + [NSCP1\ Cd^{III}] + H^+ \quad (10)$$
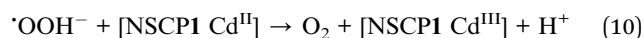
Moreover, under standard circumstances, increasing the production of $\cdot OH$ radicals using UV or ultrasonic waves might enhance the degrading effectiveness of IC dye. The following formulas demonstrate how $\cdot OH$ radicals can be produced by employing H_2O_2 and UV light.

$$h\nu + H_2O_2 \rightarrow 2\cdot OH \quad (11)$$

UV light has the ability to drive electrons from the valence band (VB) into the conduction band (CB), this can also influence the catalyst.[85] The electron transfer causes the equivalent number of positive holes (h^+) to exit the VB, as demonstrated by eqn (12). $\cdot OH$ radicals are produced when H^+ reacts with $O_2^{\cdot-}$, which is produced when e− reduces O_2 (eqn (12)–(16)) and h^+ oxidizes H_2O (eqn (17)). Attacked by $\cdot OH$ radicals, the IC dye molecules are reduced to CO_2 and H_2O as oxidation products (eqn (6) and (7)).
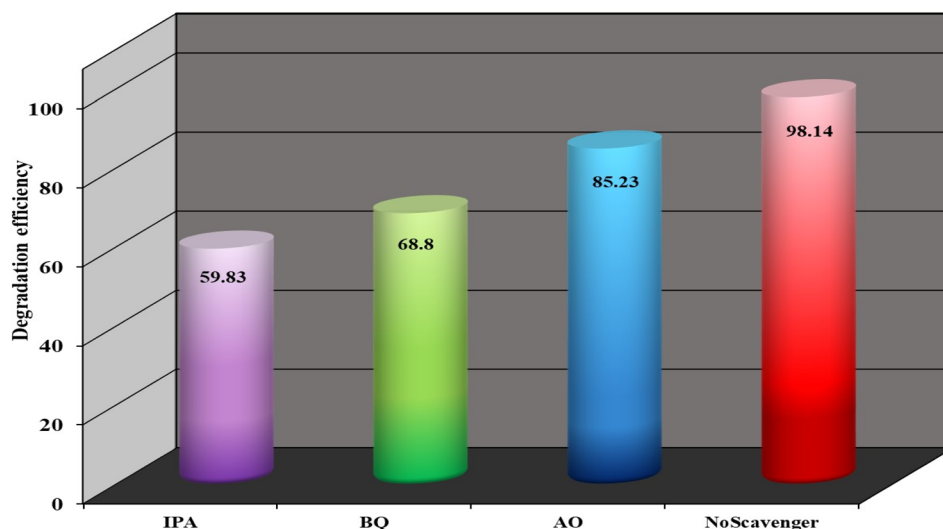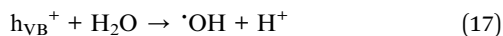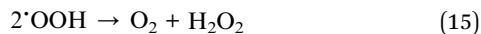

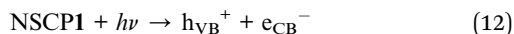Fig. 15 Impact of various scavengers on the NSCP1 catalyst-catalyzed IC dye solution degradation.

$$NSCP1 + h\nu \rightarrow h_{VB}^+ + e_{CB}^- \qquad (12)$$

$$e_{CB}^- + O_2 \rightarrow {}^\bullet O_2^- \qquad (13)$$

$${}^\bullet O_2^- + H^+ \rightarrow {}^\bullet OOH \qquad (14)$$

$$2{}^\bullet OOH \rightarrow O_2 + H_2O_2 \qquad (15)$$

$$H_2O_2 + h\nu \rightarrow 2{}^\bullet OH \qquad (16)$$

$$h_{VB}^+ + H_2O \rightarrow {}^\bullet OH + H^+ \qquad (17)$$

Using ultrasonic waves, H_2O can split [)))] according to eqn (18)–(20).

$$H_2O \xrightarrow{)))} {}^\bullet H + {}^\bullet OH \qquad (18)$$

$${}^\bullet OH + {}^\bullet OH \rightarrow H_2 + O_2 \qquad (19)$$

$${}^\bullet H + O_2 \rightarrow {}^\bullet OOH \qquad (20)$$
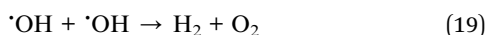
Eqn (21)–(23) state that ultrasonic radiation promoted H_2O_2 breakdown in the reaction medium.[86]

$$H_2O_2 \xrightarrow{)))} 2{}^\bullet OH \qquad (21)$$

$$e_{CB}^- + H_2O_2 \rightarrow {}^\bullet OH + OH^- \qquad (22)$$

$${}^\bullet O_2^- + H_2O_2 \rightarrow {}^\bullet OH + OH^- + O_2 \qquad (23)$$
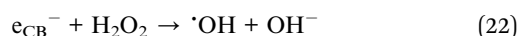
Lastly, eqn (6) and (7) show that ${}^\bullet OH$ radicals effectively oxidize IC dye to produce degradation products.

4 Conclusion

Simple, inexpensive self-assembly is used to create single crystals of supramolecular coordination polymer (SCP1), whereas ambient sonication is used to create the nano-SCP1 (NSCP1). The unique feature of SCP1 is its cyclic $[Cd_2(SCN)_2]_n$ construction blocks, which adopt the void-reducing phenomena. This structure is indicative of a non-interpenetrating network. The 3D network structure is extended by π–π stacking and H-bonds. The structures of SCP1 and NSCP1 are intriguing because they function as effective heterogeneous catalysts for the removal of organic dyes through the sophisticated advanced oxidation processes (AOC). The primary oxidative species, hydroxyl radicals, can be efficiently produced in the system with the nano-sized **1** catalyst rather than SCP1 catalyst. The pace of IC dye striate advance was significantly enhanced by UV and ultrasonic irradiation, which is also user-friendly and does not necessitate rigid reaction conditions. The tested catalysts act as heterogeneous catalysts for the efficient elimination of dyes in wastewater, comparing to other reported works,[87–90] within relatively short times mainly *via* ${}^\bullet OH$ radicals given according to (TANa) PL probing technology. The tested dye follows the Fenton process which can be considered a powerful AOP, since AOP does not need special equipment or energy input and is capable of oxidizing various organic pollutants utilizing the high oxidation potential of the ${}^\bullet OH$ radical. This method is simple and does not involve any stringent reaction conditions and can be a good alternative to other reported procedures.

Data availability

The data that support the findings of this study are available from the corresponding author upon reasonable request.

Conflicts of interest

The authors declare no conflict of interest.

Acknowledgements

References

1 J.-M. Lehn, Perspectives in Supramolecular Chemistry—From Molecular Recognition towards Molecular Information Processing and Self-Organization, *Angew. Chem. Int. Ed.*, 1990, **29**(11), 1304.

2 H.-Q. Peng, W. Z. Wu-J. Guo, Q. Li, S. Ma, C. Bucher, B. Liu, X. Ji, F. Huang and J. L. Sessler, Supramolecular polymers: Recent advances based on the types of underlying interactions, *Prog. Polym. Sci.*, 2023, **137**, 101635.

3 L. He, Y. Jiang, J. Wei, Z. Zhang, T. Hong, Z. Ren, J. Huang, F. Huang, P. J. Stang and S. Li, Highly robust supramolecular polymer networks crosslinked by a tiny amount of metallacycles, *Nat. Commun.*, 2024, **15**, 3050.

4 B. Qin, S. Liu, Z. Huang, L. Zeng, J.-F. Xu and X. Z. Qin, Closed-loop chemical recycling of cross-linked polymeric materials based on reversible amidation chemistry, *Nat. Commun.*, 2022, **13**, 7595.

5 B. Qin, S. Zhang, P. Sun, B. Tang, Z. Yin, X. Cao, Q. Chen, J.-F. Xu and X. Zhang, Tough and multi-recyclable cross-linked supramolecular polyureas *via* incorporating noncovalent bonds into main chains, *Adv. Mater.*, 2020, **32**(36), 2000096.

6 Y. Xue, C. Zhang, T. Lv, L. Qiu and F. Wang, Amplification of dissymmetry for circularly polarized photodetection by cooperative supramolecular polymerization, *Angew. Chem., Int. Ed.*, 2023, **62**, e202300972.

7 Y. Han, X. Zhang, Z. Ge, Z. Gao, R. Liao and F. Wang Han, A bioinspired sequential energy transfer system constructed *via* supramolecular copolymerization, *Nat. Commun.*, 2022, **13**, 3546.

8 F. Wang, R. Liao and F. Wang, Pathway control of π-conjugated supramolecular polymers by incorporating

donor-acceptor functionality, *Angew. Chem., Int. Ed.*, 2023, **62**, e202305827.

9 X. Tang, Z. Huang, H. Chen, Y. Kang, J.-F. Xu and X. Zhang, Supramolecularly catalyzed polymerization: from consecutive dimerization to polymerization, *Angew. Chem., Int. Ed.*, 2018, **57**(28), 8545.

10 G. Sinawang, M. Osaki, Y. Takashima, H. Yamaguchi and A. Harada, Supramolecular self-healing materials from non-covalent cross-linking host–guest interactions, *Chem. Commun.*, 2020, **56**, 4381.

11 S. E. H. Etaiw, D. M. Abd El-Aziz, E. M. Shalaby and I. Elzeny, X-ray structure of host-guest nanosized organotin supramolecular coordination polymer based on cobalt cyanide and quinoxaline as an efficient catalyst for treatment of wastewater, *Appl. Organomet. Chem.*, 2020, **34**(4), e5521.

12 S. E. H. Etaiw, D. M. Abd El-Aziz and I. Elzeny, Nano-architecture cobalt (III) supramolecular coordination polymer based on host-guest recognition as an effective catalyst for phenolic degradation and chemical sensor, *J. Organomet. Chem.*, 2020, **921**, 121397.

13 Y. Deng, Q. Zhang, B. L. Feringa, H. Tian and D.-H. Qu, Toughening a Self-healable supramolecular polymer by ionic cluster-enhanced iron-carboxylate complexes, *Angew. Chem., Int. Ed.*, 2020, **59**, 5278.

14 M. C. Gonzalez, N. Alegret, A. M. Fracaroli, D. Mantione, G. G. González, R. Del Olmo, K. Tashiro, L. C. Tomé, M. L. Picchio and D. Mecerreyes, Mixed conductive, injectable, and fluorescent supramolecular eutectogel composites, *Angew. Chem., Int. Ed.*, 2023, **62**(26), e202301489.

15 Y.-K. Tian, Y.-G. Shi, Z.-S. Yang and F. Wang, Responsive Supramolecular Polymers Based on the Bis [alkynylplatinum(II)] Terpyridine Molecular Tweezer/Arene Recognition Motif, *Angew. Chem., Int. Ed.*, 2014, **53**(24), 6090.

16 P.-Y. Gu, Y. Chai, H. Hou, G. Xie, Y. Jiang, Q.-F. Xu, F. Liu, P. D. Ashby, J.-M. Lu and T. P. Russell, Stabilizing liquids using interfacial supramolecular polymerization, *Angew. Chem., Int. Ed.*, 2019, **58**(35), 12112.

17 F. Tom, A. de Greef and E. W. Meijer, supramolecular polymers, *Nature*, 2008, **453**, 171–173.

18 X. Yan, F. Wang, B. Zheng and F. Huang, Stimuli-responsive supramolecular polymeric materials, *Chem. Soc. Rev.*, 2012, **41**, 6042.

19 S. Raza, X. Li, F. Soyekwo, D. Liao, Y. Xiang and C. Liu, A comprehensive overview of common conducting polymer-based nanocomposites; Recent advances in design and applications, *Eur. Polym. J.*, 2021, **160**(5), 110773.

20 S. Zhang, A. M. Bellinger, D. L. Glettig, R. Barman, Y.-A. L. Lee, J. Zhu, C. Cleveland, V. A. Montgomery, L. Gu, L. D. Nash, D. J. Maitland, R. Langer and G. Traverso, A pH-responsive supramolecular polymer gel as an enteric elastomer for use in gastric devices, *Nat. Mater.*, 2015, **14**, 1065.

21 A. Campanella, D. Döhler and W. H. Binder, Self-healing in supramolecular polymers, Macromol, *Rapid Commun.*, 2018, **39**(17), 1700739.

22 A. Winter and U. S. Schubert, Synthesis and characterization of metallo-supramolecular polymers, *Chem. Soc. Rev.*, 2016, **45**, 5311.

23 H. R. Marsden and A. Kros, Self-assembly of coiled coils in synthetic biology: inspiration and progress, *Angew. Chem., Int. Ed.*, 2010, **49**, 2988.

24 P. J. Yoo, K. T. Nam, J. Qi, S.-K. Lee, J. Park, A. M. Belcher and P. T. Hammond, Spontaneous assembly of viruses on multilayered polymer surfaces, *Nat. Mater.*, 2006, **5**, 234.

25 G. M. Whitesides and B. Grzybowski, Self-assembly at all scales, *Science*, 2002, **295**, 2418.

26 I. Ahmed, X. Wang, N. Boualili, H. Xu, R. Farha, M. Goldmann and L. Ruhlmann, Photocatalytic synthesis of silver dendrites using electrostatic hybrid films of porphyrin–polyoxometalate, *Appl. Catal., A*, 2012, **447–448**, 89.

27 S. Ling, D. L. Kaplan and M. J. Buehler, Nanofibrils in nature and materials engineering, *Nat. Rev. Mater.*, 2018, **3**(4), 18016.

28 P. Zou, W.-T. Chen, T. Sun, Y. Gao, L.-L. Li and H. Wang, Recent advances: peptides and self-assembled peptide-nanosystems for antimicrobial therapy and diagnosis, *Biomater. Sci.*, 2020, **8**, 4975.

29 K. Gvozden, S. N. Ratajczak, A. G. Orellana, E. Kentzinger, U. Rücker, J. K. G. Dhont, C. De Michele and E. Stiakaki, Self-assembly of all-DNA rods with controlled patchiness, *Small*, 2022, **18**, 2104510.

30 S. K. Bhangu, G. Bocchinfuso, M. Ashokkumar and F. Cavalieri, Sound-driven dissipative self-assembly of aromatic biomolecules into functional nanoparticles, *Nanoscale Horiz.*, 2020, **5**, 553.

31 A. Bayaguud, K. Chen and Y. Wei, Controllable synthesis of polyoxovanadate-based coordination polymer nanosheets with extended exposure of catalytic sites, *Nano Res.*, 2016, **9**, 3858.

32 R. Horikoshi, T. Mochida, N. Maki, S. Yamada and H. Moriyama, Coordination polymer complexes of 4,4′-dipyridyldisulfide and AgX (X = PF_6^-, ClO_4^-, OTs^-, NO_3^-, BF_4^-) with twisted rhomboid networks, 2-D sheets, and 1-D chain structures, *J. Chem. Soc., Dalton Trans.*, 2002, 28.

33 A. Valipour, B. Mirtamizdoust, M. Ghaedi, F. Taghizadeh and P. Talemi, Hemidirected Coordination Sphere on Novel Lead(II) Nano Coordination Polymer: Synthesis, Structural Characterization and DFT Calculation of [Pb(p-2-einh)ClO_4(MeOH)$_2$]$_n$, *J. Inorg. Organomet. Polym.*, 2016, **26**, 197.

34 G.-Q. Zhong, D. Li and Z.-P. Zhang, Hydrothermal synthesis, crystal structure and magnetic property of a homodinuclear ternary coordination polymer of nickel(II), *Polyhedron*, 2016, **111**, 11.

35 K. Akhbari and A. Morsali, Mechanochemical synthesis and characterization of kinetically and thermodynamically stable polymorphs of a lead(II) coordination polymer, *Inorg. Chim. Acta*, 2015, **429**, 109.

36 I. PerezF, E. S Larrea, B. Bazán, G. Barandika, M. K. Urtiaga and M. I. Arriortua, Ionothermal Synthesis of Cadmium Coordination Polymers: Ionic Liquid Effects on the

Synthesis, Structural, and Thermal Characterization, *Molecules*, 2019, **24**(22), 4059.

37 S. E. H. Etaiw, D. M. Abd El-Aziz, E. M. Shalaby and I. Elzeny, X-ray structure of host-guest nanosized organotin supramolecular coordination polymer based on cobalt cyanide and quinoxaline as an efficient catalyst for treatment of wastewater, *Appl. Organomet. Chem.*, 2020, **34**(4), e5521.

38 B. Souri, A. R. Rezvani, S. Abbasi, P. Hayati and R. Centore, An investigation on the morphology of a new coordination polymer *via* change effective factors based on eco-friendly sonochemical synthesis; new precursor for the preparation of cadmium(II) oxide, *Inorg. Chim. Acta*, 2019, **498**, 119134.

39 B. Liu, Y.-C. Qiu, G. Peng and H. Deng, In situ solvothermal syntheses of a heteronuclear copper(I)-alkaline metallic tetrazole-based coordination polymer, *CrystEngComm*, 2010, **12**, 270.

40 S. E. H. Etaiw, T. A. Fayed, D. M. Abd El-Aziz and H. M. Khatab, Ultrasound-assisted nano scaled supramolecular coordination polymer as an efficient recyclable catalyst for photocatalytic degradation of dye pollutants, *Appl. Organomet. Chem.*, 2020, **34**(2), e5301.

41 S. E.-d. H. Etaiw and H. Marie, Sono chemical nanostructure of Mn(II) supramolecular complex: X-ray structure, sensing and photocatalytic properties, *Sens. Actuators, B*, 2019, **290**, 631.

42 M. J. S. Fard, P. Hayati, A. Masoudiasl and J. Janczak, A facile route for the synthesis of new 1D copper(II) coordination polymer as precursors for preparation of nano structures: Crystallography and Hirshfeld surface analysis, *J. Mol. Struct.*, 2020, **1200**, 127020.

43 M. Alikhani, M. Hakimi, K. Moeini, V. Eigner and M. Dusek, Synthesis, Characterization and Thermal Studies of a Nanosized 1D l-Arginine/Copper(II) Coordination Polymer by Sonochemical Method: A New Precursor for preparation of copper(II) oxide nanoparticles, *J. Inorg. Organomet. Polym. Mater.*, 2020, 2907.

44 D. Klarić, V. Pilepić, D. Kontrec, A. Budimir and N. Galić, Aluminum(III) complexes of aroylhydrazones derived from nicotinic acid hydrazide: MS, UV-Vis and DFT study, *J. Coord. Chem.*, 2024, **77**, 805.

45 N. S. Awwad, H. A. Ibrahium, A. A. Shati, M. Y. Alfaifi, Y.-H. Ju and A. E. Fazarym, Nicotine metal complexes: synthesis, characterization and bioactivities of some main group and some transition metals, *Bull. Chem. Soc. Ethiop.*, 2020, **34**(3), 501.

46 Q. Yang, J.-P. Zhao, B.-W. Hu, X.-F. Zhang and X.-H. Bu, New Manganese(II) Azido Coordination Polymers with Nicotinic/Isonicotinic Acids as Coligands: Synthesis, Structure, and Magnetic Properties, *Inorg. Chem.*, 2010, **49**, 3746.

47 W. I. Liu, O. Malekahmadi, S. A. Bagherzadeh, M. Ghashang, A. Karimipour, S. Hasani, I. Tlili and M. Goodarzi, A novel comprehensive experimental study concerned graphene oxide nanoparticles dispersed in water: synthesise, characterisation, thermal conductivity measurement and present a new approach of RLSF neural network, *Int. Commun. Heat Mass Tran.*, 2019, **109**, 104333.

48 H. Karami, S. P. Zare, M. Shanbedi, H. Eshghi, A. Dashtbozorg, A. Akbari, E. Mohammadian, M. Heidari, A. Z. Sahin and C. B. Teng, The thermophysical properties and the stability of nanofluids containing carboxyl-functionalized graphene nano-platelets and multi-walled carbon nanotubes, *Int. Commun. Heat Mass Tran.*, 2019, **108**, 104302.

49 I. M. Mahbubul, R. Saidur, M. A. Amalina and M. E. Niza, Influence of ultrasonication duration on rheological properties of nanofluid: an experimental study with alumina–water nanofluid, *Int. Commun. Heat Mass Tran.*, 2016, **76**, 33.

50 M. Noroozi, S. Radiman and A. Zakaria, Influence of sonication on the stability and thermal properties of Al2O3 nanofluids, *J. Nanomater.*, 2014, 612417.

51 M. Leena and S. Srinivasan, Synthesis and ultrasonic investigations of titanium oxide nanofluids, *J. Mol. Liq.*, 2015, **206**, 103.

52 A. Ajmal, I. Majeed, R. N. Malik, H. Idriss and M. A. Nadeem, Principles and mechanisms of photocatalytic dye degradation on TiO_2 based photocatalysts: a comparative overview, *RSC Adv.*, 2014, **4**(70), 37003.

53 A. Ayati, M. N. Shahrak, B. Tanhaei and M. Sillanp, Emerging adsorptive removal of azo dye by metal–organic frameworks, *Chemosphere*, 2016, **160**, 30.

54 R. Kant, Textile dyeing industry an environmental hazard, *Nat. Sci.*, 2012, **4**(1), 22.

55 M. Zhu, L. Lee, H. Wang and Z. Wang, Removal of an anionic dye by adsorption/precipitation processes using alkaline white mud, *J. Hazard. Mater.*, 2007, **149**(3), 735.

56 M. Wang, J. Ioccozia, L. Sun, C. Lin and Z. Lin, Correction: Inorganic-modified semiconductor TiO_2 nanotube arrays for photocatalysis, *Energy Environ. Sci.*, 2014, 7, 2182.

57 S. E. H. Etaiw and S. N. Abdou, Long Chain Aliphatic Diamine as Template for the Construction of Host–Guest Copper–Cyanide 3D-Network, *J. Inorg. Organomet. Polym. Mater.*, 2017, **27**, 1901.

58 Y. Bai, W. L. Shang, D. B. Dang, J. D. Sun and H. Gao, Synthesis, crystal structure and luminescent properties of one coordination polymer of cadmium(II) with mixed thiocyanate and hexamethylenetetramine ligands, *Spectrochim. Acta, Part A*, 2009, **72**, 407.

59 A. Barbieri, G. Accorsi and N. Armaroli, Luminescent complexes beyond the platinum group: the d^{10} avenue, *Chem. Commun.*, 2008, **19**, 2185.

60 B. D. Stubbert, J. Vela, W. W. Brennessel and P. L. Holland, A Sulfide-Bridged Diiron(II) Complex with a *cis*-N_2H_4 Ligand, *Z. Anorg. Allg. Chem.*, 2013, **639**(8–9), 1351.

61 S. E. H. Etaiw and M. M. El-bendary, Metal-Organic Framework Constructed by Copper(I) Cyanide and Ethyl Isonicotinate Through Hydrogen Bonding, *J. Inorg. Organomet. Polym.*, 2010, **20**, 739.

62 M. M. Chamberlain and J. C. Bailer, The Infrared Spectra of Some Thiocyanato-cobalt Ammines, *J. Am. Chem. Soc.*, 1959, **81**(24), 6412.

63 S. Ilhan, H. Temel, I. Yilmaz and M. Sekerci, Synthesis, structural characterization and electrochemical studies of

new macrocyclic Schiff base containing pyridine head and its metal complexes, *J. Organomet. Chem.*, 2007, **692**(18), 3855.

64 V. B. Rana, D. P. Singh, P. Singh and M. P. Teotia, Divalent nickel, cobalt and copper complexes of tetradentate N$_6$ macro cyclic ligands, *Transition Met. Chem.*, 1981, **6**, 36.

65 H. H. Jaffé and M. Orchin, *Theory and Applications of Ultraviolet Spectroscopy*, Wiley, New York, 5th edn, 1970.

66 F. A. Cotton, G. Wilkinson, C. A. Murillo and M. Bochmann, *Advanced Inorganic Chemistry*, Wiley, New York, 6th edn, 1999.

67 T. T. Li, Z. Z. Wen, S. L. Cai and S. R. Zheng, Construction of four d^{10} coordination polymers containing binuclear rings as building blocks from 4′-(2H-tetrazol-5-yl)biphenyl-4-carboxylic acid, *J. Coord. Chem.*, 2016, **69**(6), 976.

68 K. Maity and K. Biradha, Role of Anions in the Formation of Multidimensional Coordination Polymers: Selective Separation of Anionic Toxic Dyes by 3D-Cationic Framework and Luminescent Properties, *Cryst. Growth Des.*, 2016, **16**(5), 3002.

69 B. Valeur, *Molecular Fluorescence Principles and Applications*, Wiley, Weinheim, 2002, p. 59.

70 Q. Q. Li, Y. F. Kang, C. Y. Ren, G. P. Yang, Q. Liu, P. Liu and Y. Y. Wang, Reaction-controlled assemblies and structural diversities of seven Co(ii)/Cu(ii) complexes based on a bipyridine-dicarboxylate N-oxide ligand, *CrystEngComm*, 2015, **17**, 775.

71 Y. Sun, S. Zhao, H. Ma, Y. Han, K. Liu and L. Wang, Positional isomerism-driven two 3D pillar-layered metal-organic frameworks: Syntheses, topological structures and photoluminescence properties, *J. Solid State Chem.*, 2016, **238**, 284.

72 S. E. H. Etaiw, S. A. Amer and M. M. El-Bendary, Luminescence and catalytic activity of mixed valence copper cyanide 3D-supramolecular coordination polymer containing 1,10-phenathorline molecule, *J. Inorg. Organomet. Polym.*, 2011, **21**, 662.

73 G. H. Wei, J. Yang, J. F. Ma, Y. Y. Liu and S. L. Li, Syntheses, structures and luminescent properties of zinc(ii) and cadmium(ii) coordination complexes based on new bis(imidazolyl)ether and different carboxylate ligands, *Dalton Trans.*, 2008, **13**, 3080.

74 L. Zhang, Z.-J. Li, Q.-P. Lin, Y.-Y. Qin, J. Zhang, P.-X. Yin, J.-K. Cheng and Y.-G. Yao, Synthesis, Structure, and Luminescent Properties of Hybrid Inorganic−Organic Framework Materials Formed by Lead Aromatic Carboxylates: Inorganic Connectivity Variation from 0D to 3D, *Inorg. Chem.*, 2009, **48**(14), 6517.

75 X. Liu, Z. Xiao, A. Huang, W. Wang, L. Zhang, R. Wang and D. Sun, Crystal structures, topological analysis and luminescence properties of three coordination polymers based on a semi-rigid ligand and N-donor ligand linkers, *New J. Chem.*, 2016, **40**, 5957.

76 K. Y. Zou, Q. Zou, T. Han, Y. C. Liu, J. J. Wang, X. Zhang and Z. X. Li, J. Anion-dependent construction of a series of fluorescent coordination polymers based on 1D zinc∩4,4′-bis(imidazole-1-yl)-biphenyl substrates, *J. Solid State Chem.*, 2016, **235**, 85.

77 S. F. A. Kettle, *Chapter 5: Stability of Coordination Compounds: Physical Inorganic Chemistry*, Springer-Verlag, Berlin, Heidelberg, 1996, p. 73.

78 H. Irving and R. J. P. Williams, The stability of transition metal complexes, *J. Chem. Soc.*, 1953, 3192.

79 Z. Yu and S. S. Chuang, Probing methylene blue photocatalytic degradation by adsorbed ethanol with *in situ* IR, *J. Phys. Chem. C*, 2007, **111**(37), 13813.

80 J. Yu, Q. Xiang and M. Zhou, Preparation, characterization and visible-light-driven photocatalytic activity of Fe-doped titania nanorods and first-principles study for electronic structures, *Appl. Catal., B*, 2009, **90**(3–4), 595.

81 A. Farrokhi, M. Jafarpour and M. Alipour, Solar-driven advanced oxidation process catalyzed by metal–organic frameworks for water depollution, *Polyhedron*, 2019, **170**, 325.

82 S. E. H. Etaiw, T. A. Fayed, D. M. A. El-Aziz and H. M. Khattab, Self-assembly and Nano scaled Ni (II) Coordination Complex as an Efficient Catalyst and Luminescent Sensor, *J. Inorg. Organomet. Polym. Mater.*, 2021, **31**(4), 1621.

83 S. E. H. Etaiw, R. S. Farag, H. Marie and F. A. Elsharqawy, Crystal structure and sonochemical nanosized synthesizing of diaquo-bis-(pyrazine-2-carboxylato) copper (II) complex: Sensing and photocatalytic activity, *Solid State Sci.*, 2020, **102**, 106160.

84 W. Bae, S. Lee and G. Ko, Evaluation of predominant reaction mechanisms for the Fenton process in textile dyeing wastewater treatment, *Water Sci. Technol.*, 2004, **49**(4), 91.

85 W. Sun, S. Meng, S. Zhang, X. Zheng, X. Ye, X. Fu and S. Chen, Insight into the transfer mechanisms of photogenerated carriers for heterojunction photocatalysts with the analogous positions of valence band and conduction band: a case study of ZnO/TiO2, *J. Phys. Chem. C*, 2018, **122**(27), 15409.

86 K. Zhang, N. Gao, Y. Deng, T. F. Lin, Y. Ma, L. Li and M. Sui, Degradation of bisphenol-A using ultrasonic irradiation assisted by low-concentration hydrogen peroxide, *J. Environ. Sci.*, 2011, **23**(1), 31.

87 P. E. Umoru, I. U. Nkole and T. T. Ezeh, Degradation of indigo carmine dye with peroxydisulphate ion in aqueous sulphuric acid phase: Kinetic study, *Int. J. Chem. Kinet.*, 2024, **56**(6), 339.

88 M. S. l Sha, H. Anwar, F. N. Musthafa, H. Al-Lohedan, S. Alfarwati, J. R. Rajabathar, J. K. Alahmad, J.-J. Cabibihan, M. Karnan and K. K. Sadasivuni, Photocatalytic degradation of organic dyes using reduced graphene oxide (rGO), *Sci. Rep.*, 2024, **14**, 3608.

89 B. Viswanathan, Photocatalytic Degradation of Dyes: An Overview, *Curr. Catal.*, 2018, 7, 1.

90 J. S. G. Neto, S. Satyro, E. M. Saggioro and M. Dezotti, Investigation of mechanism and kinetics in the TiO$_2$ photocatalytic degradation of Indigo Carmine dye using radical scavengers, *Int. J. Environ. Sci. Technol.*, 2021, **18**, 163.